Single top quark production in $e\gamma$ collisions and testing technicolor models

Xuelei Wang
Department of Physics, Tsinghua University, Beijing 100084, China
and Physics Department, Henan Normal University, Xinxiang Henan 453002, China

Yu-Ping Kuang and Hong-Yi Zhou
China Center of Advanced Science and Technology (World Laboratory), P.O. Box 8730, Beijing 100080, China
*and Institute of Modern Physics, Tsinghua University, Beijing 100084, China**

Hua Wang and Ling Zhang
Department of Physics, Tsinghua University, Beijing 100084, China
(Received 2 November 1998; revised manuscript received 25 January 1999; published 20 May 1999)

We study the single top quark production process $e^+\gamma\to t\bar{b}\bar{\nu}_e$ in various kinds of technicolor models in high energy $e\gamma$ collisions at the future e^+e^- linear colliders. It is shown that if there is a certain charged pseudo-Goldstone-boson (PGB) coupling to $t\bar{b}$, the $t\bar{b}$-channel PGB contribution is dominant, but the situation is quite different from that in the neutral channel $\gamma\gamma\to t\bar{t}$ due to the destructive nature of different amplitudes. At the DESY linear collider TESLA, the event rates in models with $t\bar{b}$-channel PGB contributions, such as the top-color-assisted technicolor model, etc., are experimentally measurable. The $e^+\gamma\to t\bar{b}\bar{\nu}_e$ process provides a feasible test of technicolor models with $t\bar{b}$-channel charged PGB contributions. [S0556-2821(99)04511-7]

PACS number(s): 14.65.Ha, 12.15.Lk, 12.60.Nz

I. INTRODUCTION

So far the most unclear part of the standard model is its symmetry breaking sector. Probing the electroweak symmetry breaking mechanism will be one of the most important tasks at future high energy colliders. Dynamical electroweak symmetry breaking, for example technicolor type theories, is an attractive idea that it avoids the shortcomings of triviality and unnaturalness arising from the elementary Higgs field. The simplest QCD-like extended technicolor model [1] leads to a too large oblique correction S parameter [2], and is already ruled out by the recent CERN e^+e^- collider LEP precision electroweak measurement data [3,4]. Various improvements have been made to make the predictions consistent with the LEP precision measurement data and even to give possible dynamical explanation of the heaviness of the top quark, for example the walking technicolor models [5], the Appelquist-Terning one-family model [6], the multi-scale walking technicolor models [7], the top-color-assisted technicolor models (TC2) [8,9], the non-commuting extended technicolor model [10], etc. This kind of dynamical electroweak symmetry breaking theory is one of the important candidates of the electroweak symmetry breaking mechanism. Because of the strong interaction nature, it is hard to make precise calculations in such dynamical electroweak symmetry breaking theories. However, there are some characteristic features in this kind of models, for instance the prediction for certain pseudo-Goldstone bosons (PGB's) in the few hundred GeV region. It is thus interesting to find experimentally measurable processes which are sensitive to the PGB's to test this kind of models.

The top quark is the heaviest particle yet experimentally discovered and its mass 175 GeV [11] is close to the electroweak symmetry breaking scale 246 GeV. Thus processes containing the top quark may be sensitive to the electroweak symmetry breaking mechanism, and top quark productions at high energy colliders can be good processes for probing the electroweak symmetry breaking mechanism. There have been many papers studying the test of new physics via top quark productions at high energy colliders in the literatures. For instance, the model-independent studies in the effective Lagrangian formalism have been given in Refs. [12–14], supersymmetric corrections to top quark productions at hadron colliders and electron (photon) linear colliders (LC) have been studied in Ref. [15], top quark pair productions at hadron colliders and photon colliders in various technicolor models have been studied in Refs. [16,17]. Recently, there has been a lot of interests in studying single top quark productions which provides a sensitive measurement of the Wtb coupling [18]. There have been many papers studying single top quark productions in new physics models [19], and also model-independent study as well [14]. In Refs. [16,17] it is shown that, in the $t\bar{t}$ productions, once there is a neutral PGB coupling strongly to $t\bar{t}$, the $t\bar{t}$-channel PGB contribution is large and dominant over all other loop corrections, and thus such processes can be sensitive tests of the neutral PGB effects. In this paper, we shall study the $e^+\gamma\to t\bar{b}\bar{\nu}_e$ process at the high energy $e\gamma$ colliders in various technicolor models, and we shall show that this process is sensitive to the $t\bar{b}$-channel charged PGB effects if there is certain

*Mailing address.

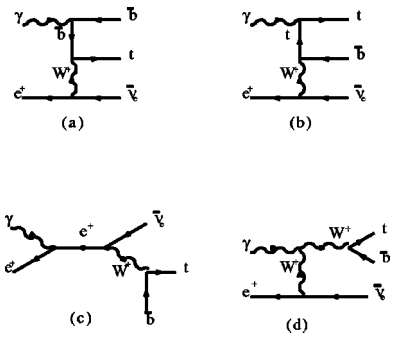

FIG. 1. Tree-level Feynman diagrams contributing from various technicolor models to the process $e^+\gamma\to t\bar{b}\nu_e$. The dashed lines denote color-singlet technipions or top-pions.

charged PGB(s) coupling strongly to $t\bar{b}$.[1] We shall see that the $e^+\gamma\to t\bar{b}\nu_e$ process at the $e\gamma$ colliders based on the LC, especially the DESY TeV Energy Superconducting Linear Accelerator (TESLA), is a feasible test of the charged PGB effects, and *the situation is quite different from that in the neutral* $\gamma\gamma\to t\bar{t}$ *channel due to the large mass difference between the top quark and the bottom quark and the destructive nature of different amplitudes*. Of special interest is the test of the charged top-pion effect in the TC2 models. The recent Fermilab Collider Detector at (CDF) data on $t\bar{t}$ production at the Fermilab Tevatron show that the branching fraction for a top quark decaying into a final state e or μ is consistent with the tree-level standard model prediction up to a certain uncertainty [20]. Future improved experiments may lead to more precise conclusion. As has been discussed in Ref. [8] that this means a charged top-pion lighter than the top quark may not be favored, and a charged top-pion heavier than the top quark will have a broad width so that it is difficult to detect. Our result shows that the $e^+\gamma\to t\bar{b}\nu_e$ process at the DESY TESLA provides a possible test of the charged top-pion effect.

This paper is organized as follows. In Sec. II, we shall present the calculations of the $e^+\gamma\to t\bar{b}\nu_e$ production amplitudes in several currently improved technicolor models. We take the TC2 model as a typical example of models containing charged PGB's strongly coupling to $t\bar{b}$. The numerical results of the cross sections will be presented in Sec. III, and Sec. IV is a concluding remark.

II. THE $e^+\gamma\to t\bar{b}\bar{\nu}_e$ PRODUCTION AMPLITUDES

The tree-level standard model contributions to the process

$$e^+ + \gamma \to t + \bar{b} + \bar{\nu}_e \tag{1}$$

[1]The present study is different from that in Ref. [14] in the following sense. Reference [14] studied single top quark production in $e\gamma$ collision at tree level in the standard model and with the consideration of possible model-independent anomalous Wtb couplings but without considering the contributions from light PGB(s). Our present study takes account of one-loop corrections and the light PGB(s) contributions in various kinds of technicolor models which are shown to be significant.

TABLE I. The masses m_{Π_t}, m_Π and the decay constants F_{Π_t}, F_Π of the top-pion and the technipion in the TC2-I and TC2-II models.

Model	top-pion Π_t		technipion Π	
	m_{Π_t} (GeV)	F_{Π_t} (GeV)	m_Π (GeV)	F_Π (GeV)
TC2-I	150–380	50	100–220	123
TC2-II	150–380	50	100–220	40

are shown in Fig. 1(a)–Fig. 1(d). The momenta of these particles will be denoted by p_{e^+}, p_γ, p_t, $p_{\bar{b}}$ and $p_{\bar{\nu}}$, respectively. In high energy processes, the effects of m_e is negligibly small. Thus we neglect it in the following calculations. We take the unitary gauge. The obtained tree-level standard model amplitude is explicitly

$$\mathcal{M}_0 = \mathcal{M}_0^{(1a)} + \mathcal{M}_0^{(1b)} + \mathcal{M}_0^{(1c)} + \mathcal{M}_0^{(1d)}, \tag{2}$$

where

$$\mathcal{M}_0^{(1a)} = -\frac{8i\sqrt{2\pi\alpha}M_W^2 G_F}{6} G(p_{\bar{b}} - p_\gamma; m_b) \times G(p_{e^+} - p_{\bar{\nu}}; M_W)\bar{u}_t \gamma_\mu L(\not{p}_{\bar{b}} - \not{p}_\gamma + m_b)\not{\epsilon} v_b \times T^W_{\mu\lambda}(p_{e^+} - p_{\bar{\nu}})\bar{v}_e \gamma_\lambda L v_{\nu_e}, \tag{3}$$

$$\mathcal{M}_0^{(1b)} = -\frac{8i\sqrt{2\pi\alpha}M_W^2 G_F}{3} G(p_t - p_\gamma; m_t) \times G(p_{e^+} - p_{\bar{\nu}}; M_W)\bar{u}_t \not{\epsilon}(\not{p}_t - \not{p}_\gamma + m_t)\gamma_\mu L v_b \times T^W_{\mu\lambda}(p_{e^+} - p_{\bar{\nu}})\bar{v}_e \gamma_\lambda L v_{\nu_e}, \tag{4}$$

$$\mathcal{M}_0^{(1c)} = -\frac{8i\sqrt{2\pi\alpha}M_W^2 G_F}{2} G(p_{e^+} + p_\gamma; 0) \times G(p_t + p_{\bar{b}}; M_W)\bar{u}_t \gamma_\rho L v_b T^W_{\rho\sigma}(p_t + p_{\bar{b}}) \times \bar{v}_e \not{\epsilon}(\not{p}_{e^+} + \not{p}_\gamma)\gamma_\sigma L v_{\nu_e}, \tag{5}$$

$$\mathcal{M}_0^{(1d)} = -\frac{8i\sqrt{2\pi\alpha}M_W^2 G_F}{2} G(p_t + p_{\bar{b}}; M_W) \times G(p_{e^+} - p_{\bar{\nu}}; M_W)\bar{u}_t \gamma_\rho L v_b T^W_{\rho\sigma}(p_t + p_{\bar{b}}) \times [\epsilon_\mu (p_{e^+} - p_{\bar{\nu}} - p_\gamma)_\sigma + \epsilon_\sigma (p_t + p_{\bar{b}} + p_\gamma)_\mu - g_{\mu\sigma}(p_{e^+} - p_{\bar{\nu}} + p_t + p_{\bar{b}})\cdot\epsilon] \times T^W_{\mu\lambda}(p_{e^+} - p_{\bar{\nu}})\bar{v}_e \gamma_\lambda L v_{\nu_e}, \tag{6}$$

with the propagator

$$G(p; M) \equiv \frac{1}{p^2 - M^2}, \tag{7}$$

the tensor

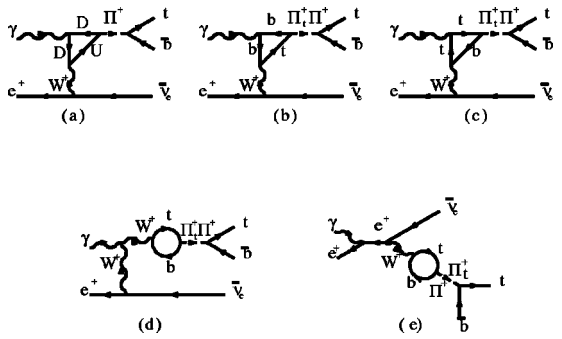

FIG. 2. One-loop Feynman diagrams for resonance contributing from various technicolor models to the process $e^+\gamma\to t\bar{b}\nu_e$. The dashed lines denote color-singlet technipions or top-pions.

$$T^W_{\rho\sigma}(p_i+p_j)\equiv g_{\rho\sigma}-\frac{(p_i+p_j)_\rho(p_i+p_j)_\sigma}{M_W^2}, \tag{8}$$

and $L\equiv\frac{1}{2}(1-\gamma_5)$, $R\equiv\frac{1}{2}(1+\gamma_5)$. In Eq. (7), M stands for the mass of the particle.

The technicolor and top-color contributions to this process depend on the models. We take certain models as typical examples.

A. The TC2 models

We first consider the TC2 model. There have been improvements of the TC2 model [9] to overcome some shortcomings of the original model and make it more realistic [21,9]. Since the purpose of this paper is to test the characteristic effects of the charged PGB's, we are not considering the delicate refinements and shall simply take the original TC2 model (it will be referred to as model TC2-I in this paper) [8] and the top-color-assisted multiscale technicolor model (it will be referred to as model TC2-II in this paper) [28,16,17] as typical examples.

In model TC2-I, there is a charged top-pion Π_t^+ in the top-color sector with mass roughly around 200 GeV and decay constant $F_{\Pi_t}=50$ GeV [8]. We take its technicolor sector to be the standard extended technicolor model, thus there is a charged technipion Π^+ from the technicolor sector with mass roughly around 100 GeV (or larger) and decay constant $F_\Pi=123$ GeV [1]. Model TC2-II [28,16,17] differs from model TC2-I only by its extended technicolor sector which is taken to be the multiscale walking technicolor model [7] in which the technipion decay constant is $F_\Pi=40$ GeV [7] rather than 123 GeV. To see the influence of the PGB masses on the production cross section, we take m_{Π_t} and m_Π to vary in certain ranges: 150 GeV$\leqslant m_{\Pi_t}\leqslant$380 GeV and 100 GeV$\leqslant m_\Pi\leqslant$220 GeV. The values of these parameters are summarized in Table I.

1. Model TC2-I

As we have seen from Refs. [22,17] that the technicolor and top-color gauge boson contributions to the Wtb vertex and the direct technicolor dynamics contribution to the $t\bar{t}$ production rate are only of the order of a few percent which

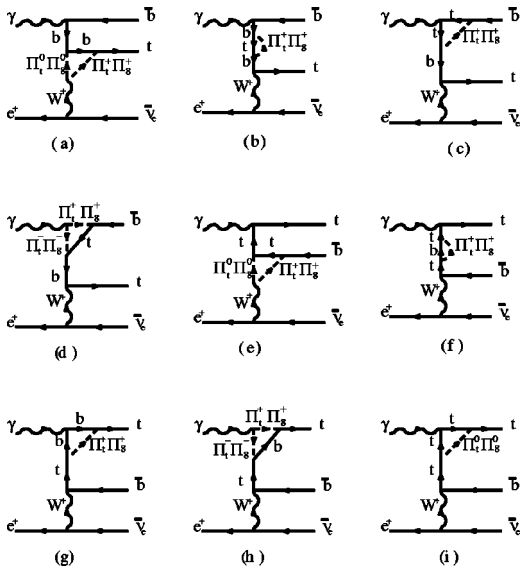

FIG. 3. One-loop Feynman diagrams for nonresonance contributing from various technicolor models to the process $e^+\gamma\to t\bar{b}\nu_e$. The dashed lines denote color-singlet technipions or top-pions.

are much smaller than the resonance enhanced $t\bar{t}$-channel PGB contributions to the top quark pair productions [16,17]. Thus we concentrate our study to the PGB contributions in this paper.

The Feynman diagrams for PGB contributions to the process $e^+\gamma\to t\bar{b}\bar{\nu}_e$ are shown in Fig. 2 and Fig. 3.[2] In Fig. 2, enhanced by the PGB resonance effects, are the most important $t\bar{b}$-channel PGB contributions. The contributions from Fig. 3, without PGB resonance enhancements, are only of the order of ordinary radiative corrections (less than 1%) and are negligibly small compared with those from Fig. 2.

The technifermion triangle loop contribution to the $\Pi^+-W^+-\gamma$ vertex [Fig. 2(a)] in extended technicolor models can be approximately evaluated [23] from the formulas for the Adler-Bell-Jackiw anomaly [24]. The result has been given in Ref. [25]. The $\Pi^+-W^+-\gamma$ coupling is

$$\frac{S_{\Pi^+W^+\gamma}}{4\pi^2F_\pi}\varepsilon_{\mu\nu\alpha\beta}\epsilon_1^\mu\epsilon_2^\nu k_1^\alpha k_2^\beta, \tag{9}$$

$$S_{\Pi^+W^+\gamma}=\frac{e^2}{2\sqrt{3}s_w}N_{TC}, \tag{10}$$

where the technicolor number is taken to be $N_{TC}=4$.

The quark triangle loops [Fig. 2(b) and Fig. 2(c)] are more complicated. They contain both the top quark and the bottom quark propagators with the masses of these quarks relatively light and significantly different. The contributions of these

[2]There are additional loop diagrams with the photon line attached to the PGB line and the external t and $\bar{b}$ lines which vanish in the approximation $m_e\approx 0$ in our calculation, so that they are not shown in Figs. 1–3.

triangle loops are thus essentially different from the result of the Adler-Bell-Jackiw anomaly, and they actually contain logarithmic ultraviolet divergences. There are no corresponding tree-level terms to absorb these divergences. However, to guarantee $U(1)_{em}$ gauge invariance, we should also take account of Fig. 2(d)–Fig. 2(e) [nonvanishing as $m_e \approx 0$] which also contain logarithmic ultraviolet divergences, and cannot be absorbed into tree-level terms. Explicit results show that these two kinds of ultraviolet divergences just cancel each other and the total result is finite as it should be. Because of the destructive nature of these two kinds of amplitudes, there is a significant cancellation between the finite corrections from these two kinds of amplitudes. This makes the charged channel $e^+\gamma \to t\bar{b}\nu_e$ very different from the neutral channel $\gamma\gamma \to t\bar{t}$, and the detection of the charged channel needs a larger integrated luminosity as we shall see in Sec. III.

To explicitly calculate the contributions of Fig. 2(b)–Fig. 2(e), we need the couplings of the technipion Π^+ and the top-pion Π_t^+ to quarks. In the original extended technicolor models without top-color, the coupling of Π^+ to quarks has been given in Ref. [25] which is

$$ic_f \frac{m_t}{F_\Pi} \bar{u}_t L u_b \Pi^+ + \text{H.c.}, \tag{11}$$

where $c_f = 1/\sqrt{6}$. In TC2 models, the extended technicolor dynamics only provides a small part of the top quark mass m_t'. For reasonable range of the parameters in TC2 models, $m_t' \sim 5-20$ GeV [8,26]. Thus the coupling of the technipion Π^+ to quarks in TC2 models can be obtained by replacing m_t by m_t' in Eq. (11), i.e.,

$$ic_f \frac{m_t'}{F_\Pi} \bar{u}_t L u_b \Pi^+ + \text{H.c.} \tag{12}$$

Similarly, the coupling of the top-pion Π_t^+ to quarks is of the following form:

$$i\frac{m_t - m_t'}{F_{\Pi_t}} \bar{u}_t L u_b \Pi_t^+ + \text{H.c.} \tag{13}$$

In the $\Pi^+(\Pi_t^+)$-propagator in Fig. 2(a)–Fig. 2(e), the time-like momentum may hit the $\Pi^+(\Pi_t^+)$-pole. So we should take into account the effects of the widths of Π^+ and Π_t^+ in the calculation. For the $\Pi^+(\Pi_t^+)$-propagator in Eq. (7), we take the complex mass term $M^2 - iM\Gamma$ instead of the simple mass term M^2 to include the effect of the width Γ of $\Pi^+(\Pi_t^+)$. The $-iM\Gamma$ term is important in the vicinity of the resonance. It is this resonance contribution that enhances the amplitudes of Fig. 2(a)–Fig. 2(e). When $M_\Pi,\ M_{\Pi_t} > m_t$, the dominant decay mode of Π^+ and Π_t^+ is $t\bar{b}$. So, in this case the widths Γ_Π and Γ_{Π_t} are

$$\Gamma_\Pi \approx \Gamma_{\Pi^+}(\Pi \to t\bar{b}) = c_f^2 \frac{m_t'^2 (m_\Pi^2 - m_t^2)^2}{16\pi F_\Pi^2 M_\Pi^3} \tag{14}$$

and

$$\Gamma_{\Pi_t} \approx \Gamma_{\Pi_t^+}(\Pi_t \to t\bar{b}) = \frac{(m_t - m_t')^2 (m_{\Pi_t}^2 - m_t^2)^2}{16\pi F_{\Pi_t}^2 M_{\Pi_t}^3}. \tag{15}$$

When $M_{\Pi_t},\ M_\Pi < m_t$, Π_t^+ and Π^+ decay dominantly into $c\bar{s}$. For small $m_b,\ m_s$, we can approximately take Γ_{Π_t} and Γ_Π to be zero.

With Eqs. (12)–(15), we can do the explicit calculation of the contributions of Fig. 2(b)–Fig. 2(e) to the amplitude. In the calculation, we take dimensional regularization and the on-shell renormalization scheme. The obtained amplitude with technicolor corrections is

$$\mathcal{M} = \mathcal{M}_0 + \Delta\mathcal{M}_{TC}^{(2a)} + \Delta\mathcal{M}_{TC}^{(2b-2e)}(\Pi^+) + \Delta\mathcal{M}_{TC}^{(2b-2e)}(\Pi_t^+) + \Delta\mathcal{M}_{TC}^{(3a-3i)}, \tag{16}$$

where the superscripts denote the corresponding Feynman diagrams in Fig. 2. The explicit formulas for $\Delta\mathcal{M}_{TC}^{(2a)}$, $\Delta\mathcal{M}_{TC}^{(2b-2e)}(\Pi^+)$, and $\Delta\mathcal{M}_{TC}^{(2b-2e)}(\Pi_t^+)$ are

$$\Delta\mathcal{M}_{TC}^{(2a)} = -c_f \frac{m_t' M_W S_{\Pi^+W^+\gamma}}{4\pi^2 F_\Pi^2} \sqrt{2\sqrt{2}G_F}\, G(p_t + p_{\bar{b}}; M_\pi) G(p_{e^+} - p_{\bar{\nu}}; M_W) \bar{u}_t L v_b \varepsilon^{\mu\nu\alpha\beta} \epsilon_\mu(p_\gamma)_\alpha (p_{e^+} - p_\nu)_\beta \times T_{\mu\lambda}^W (p_{e^+} - p_{\bar{\nu}}) \bar{v}_e \gamma_\lambda L v_{\nu_e}, \tag{17}$$

$$\Delta\mathcal{M}_{TC}^{(2b-2e)}(\Pi^+) = -ic_f \frac{m_t' M_W}{F_\Pi} \sqrt{2\sqrt{2}G_F}\, G(p_t + p_{\bar{b}}; M_\Pi) G(p_{e^+} - p_{\bar{\nu}}; M_W) \bar{u}_t L v_b [\Gamma^{(2b)\mu\nu}(\Pi) + \Gamma^{(2c)\mu\nu}(\Pi) + \Gamma^{(2d)\mu\nu}(\Pi)] \times \epsilon_\nu T_{\mu\lambda}^W (p_{e^+} - p_{\bar{\nu}}) \bar{v}_e \gamma^\lambda L v_{\nu_e} + ic_f \frac{m_t' M_W}{F_\Pi} \sqrt{8\pi\sqrt{2}G_F \alpha}\, G(p_t + p_{\bar{b}}; M_\Pi) G(p_t + p_{\bar{b}}; M_W) G(p_{e^+} + p_\gamma; 0) \times \bar{u}_t L v_b [-i\Sigma^\mu(\Pi)] T_{\mu\nu}^W (p_t + p_{\bar{b}}) \bar{v}_e \not{\epsilon}(\not{p}_{e^+} + \not{p}_\gamma) \gamma^\nu L v_{\nu_e}, \tag{18}$$

and

$$\Delta\mathcal{M}_{TC}^{(2b-2e)}(\Pi_t^+)=-i\frac{(m_t-m_t')M_W}{F_{\Pi_t}}\sqrt{2\sqrt{2}G_F}G(p_t+p_{\bar{b}};M_{\Pi_t})G(p_{e^+}-p_{\bar{\nu}};M_W)\overline{u}_tLv_b$$
$$\times[\Gamma^{(2b)\mu\nu}(\Pi_t)+\Gamma^{(2c)\mu\nu}(\Pi_t)+\Gamma^{(2d)\mu\nu}(\Pi_t)]\epsilon_\nu T^W_{\mu\lambda}(p_{e^+}-p_{\bar{\nu}})\overline{v}_e\gamma^\lambda Lv_{\nu_e}$$
$$+i\frac{(m_t-m_t')M_W}{F_{\Pi_t}}\sqrt{8\pi\sqrt{2}G_F\alpha}G(p_t+p_{\bar{b}};M_{\Pi_t})G(p_t+p_{\bar{b}};M_W)G(p_{e^+}+p_\gamma;0)\overline{u}_tLv_b$$
$$\times[-i\Sigma^\mu(\Pi_t)]T^W_{\mu\nu}(p_t+p_{\bar{b}})\overline{v}_e\not{\epsilon}(\not{p}_{e^+}+\not{p}_\gamma)\gamma^\nu Lv_{\nu_e}. \tag{19}$$

In Eqs. (18),(19) the functions $\Gamma^{(2b)}_{\mu\nu}$, $\Gamma^{(2c)}_{\mu\nu}$, $\Gamma^{(2d)}_{\mu\nu}$, and Σ_μ are given in the Appendix in terms of the standard 2-point and 3-point functions B_0, B_1 and C_0, C_{ij} of the Feynman integrals [27]. The formula for $\Delta\mathcal{M}_{TC}^{(3a-3i)}$ is quite lengthy and we are not going to show it since its contribution is only of the order of ordinary radiative corrections (less than 1%) and is negligibly small compared with those shown in Eqs. (17)–(19) which are enhanced by the PGB resonance effects.

2. Model TC2-II

In model TC2-II, the extended technicolor sector is taken to be the multiscale walking technicolor model [7] in which the technipion Π^+ is almost composed of pure techniquarks [28], Thus the relevant changes in the above formulas are

$$c_f=\frac{2}{\sqrt{6}},\quad S_{\Pi^+W^+\gamma}=\frac{e^2}{4\sqrt{3}s_w}. \tag{20}$$

The smallness of the decay constant F_Π in this model [cf. Table I] will enhance the Π^+ contribution [cf. Eqs. (17)–(19)].

B. The Appelquist-Terning one family extended technicolor model

This model is designed in which the techniquark sector respects the custodial $SU(2)$ symmetry, while the technilepton sector is custodial $SU(2)$ violating. The vacuum expectation value (VEV) F_Q of the techniquark condensate is much larger than the VEV F_L of the technilepton condensate [6]. There are 36 PGB's in this model, and the color singlet PGB's are mainly composed of technileptons which is irrelevant to the production of $t\bar{b}$. Thus in this model there are no $\Delta\mathcal{M}_{TC}^{(2a)}(\Pi^+)$ and $\Delta\mathcal{M}_{TC}^{(2b-2e)}(\Pi^+)$. The only technicolor contribution to the $e^+\gamma\to t\bar{b}\bar{\nu}_e$ is $\Delta\mathcal{M}_{TC}^{(3a-3i)}$ which is much smaller than those in Eqs. (17)–(19). Thus the cross sections in this model will be much smaller than those in the previous models.

We shall see from the numerical results in the next section that, for certain parameter range, these models can all be measured and distinguished by their $e^+\gamma\to t\bar{b}\bar{\nu}_e$ rates at the DESY TESLA.

III. THE CROSS SECTIONS

The hard photon beam of the $e^+\gamma$ collider can be obtained from laser backscattering at the e^+e^- linear collider [29]. Let $\hat{s}$ and s be the center-of-mass energies of the $e^+\gamma$ and e^+e^- systems, respectively. After calculating the cross section $\sigma(\hat{s})$ for the subprocess $e^+\gamma\to t\bar{b}\bar{\nu}_e$, the total cross section at the e^+e^- linear collider can be obtained by folding $\sigma(\hat{s})$ with the photon distribution function $f_\gamma(x)$ $(\hat{s}=xs)$

$$\sigma_{tot}=\int_{(m_t+m_b)^2/s}^{x_{max}}dx\hat{\sigma}(\hat{s})f_\gamma(x), \tag{21}$$

where

$$f_\gamma(x)=\frac{1}{D(\xi)}\left[1-x+\frac{1}{1-x}-\frac{4x}{\xi(1-x)}+\frac{4x^2}{\xi^2(1-x)^2}\right], \tag{22}$$

with [29]

$$D(\xi)=\left(1-\frac{4}{\xi}-\frac{8}{\xi^2}\right)\ln(1+\xi)+\frac{1}{2}+\frac{8}{\xi}-\frac{1}{2(1+\xi)^2}. \tag{23}$$

In Eqs. (22) and (23), $\xi=4E_e\omega_0/m_e^2$ in which m_e and E_e stand, respectively, for the incident electron mass and energy, ω_0 stands for the laser photon energy, and $x=\omega/E_e$ stands for the fraction of energy of the incident electron carried by the back-scattered photon. f_γ vanishes for $x>x_{max}=\omega_{max}/E_e=\xi/(1+\xi)$. In order to avoid the creation of e^+e^- pairs by the interaction of the incident and back-scattered photons, we require $\omega_0 x_{max}\leqslant m_e^2/E_e$ which implies that $\xi\leqslant 2+2\sqrt{2}\approx 4.8$. For the choice of $\xi=4.8$, we obtain

$$x_{max}\approx 0.83,\quad D(\xi)\approx 1.8. \tag{24}$$

In the calculation of $\sigma(\hat{s})$, instead of calculating the square of the renormalized amplitude $\mathcal{M}$ analytically, we calculate the amplitudes numerically by using the method of Ref. [30]. This greatly simplifies our calculations. Care must be taken in the calculation of the form factors expressed in terms of the standard loop integrals defined in Ref. [27]. In

TABLE II. Top-pion corrections to the $e^+\gamma\to t\bar{b}\nu_e$ production cross section $\Delta\sigma_{\Pi_t}$ and the total production cross section $\sigma=\sigma_0+\Delta\sigma_{\Pi_t}+\Delta\sigma_{\Pi}$ in model TC2-I with $m_{\Pi}=220$ GeV and various values of m_{Π_t}. The technipion corrections are negligibly small. The tree level production cross section $\sigma_0=3.25$ fb for $\sqrt{s}=0.5$ TeV, $\sigma_0=14.73$ fb for $\sqrt{s}=1.6$ TeV.

$\sqrt{s}$	$m_t'=5$ GeV			$m_t'=20$ GeV		
(TeV)	m_{Π_t} (GeV)	$\Delta\sigma_{\Pi_t}$ (fb)	σ (fb)	m_{Π_t} (GeV)	$\Delta\sigma_{\Pi_t}$ (fb)	σ (fb)
	150	0.0025	3.25	150	−0.004	3.25
	180	0.083	3.26	180	0.06	3.26
0.5	200	0.081	3.33	200	0.062	3.31
	240	0.12	3.37	240	0.096	3.35
	300	0.098	3.35	300	0.083	3.33
	380	0.058	3.31	380	0.052	3.30
	150	−0.12	14.61	150	−0.11	14.62
	180	−0.11	14.62	180	−0.099	14.63
1.6	200	0.05	14.78	200	0.039	14.77
	240	0.086	14.82	240	0.061	14.79
	300	0.082	14.81	300	0.058	14.79
	380	0.05	14.78	380	0.042	14.77

the numerical calculation, we used the formulas for the tensor loop integrals given in Ref. [27] in which the stability of the numerical calculation is poor when the scattering is forwards or backwards [31]. This problem can be avoided by taking certain kinematic cuts on the rapidity y and the transverse momentum p_T of the final states which are also needed in experimental detections. In order to compare with the corresponding results in the neutral channel, we take, in this paper, the same kinematic cuts as in Ref. [17], i.e.

$$|y|<2.5,\ \ p_T>20\ \ \text{GeV}. \tag{25}$$

The cuts will also increase the relative correction [32].

In our calculation, we take $m_t=176$ GeV, $m_b=4.9$ GeV, $M_W=80.33$ GeV, $G_F=1.19347\times10^{-5}$ $(\text{GeV})^{-2}$, $s_w^2=0.23$. The electromagnetic fine structure constant α at certain energy scale is calculated from the simple QED one-loop evolution formula with the boundary value $\alpha=1/137.04$ [33], and we will not consider the hadronic corrections here since they do not affect the conclusions in this paper to the present precision.

For estimating the event rates, we take the following integrated luminosities corresponding to a one-year-run at the DESY TESLA [34]

$$\sqrt{s}=0.5\ \ \text{TeV}:\quad \int \mathcal{L}dt\approx 500\ \ \text{fb}^{-1} \tag{26}$$

$$\sqrt{s}=0.8\ \ \text{TeV}:\quad \int \mathcal{L}dt=500\ \ \text{fb}^{-1}$$

$$\sqrt{s}=1.6\ \ \text{TeV}:\quad \int \mathcal{L}dt\geqslant 500\ \ \text{fb}^{-1}.$$

Our numerical results show that the contributions from the diagrams in Fig. 3 to the production cross section are negligibly small in all models considered in this paper. Therefore we simply ignore them.

In model TC2-I, the numerical results show that the technicolor PGB contributions to the production cross section are negligibly small compared with the contributions from the top-pion for $m_{\Pi}\lesssim 220$ GeV. In Table II, we list the correction to the production cross section $\Delta\sigma_{\Pi_t}$ (from the top-pion contributions) and the total cross section σ with 150 GeV $\leqslant m_{\Pi_t}\leqslant 380$ GeV, $m_t'=5,\ 20$ GeV at the 0.5 and 1.6 TeV LC. We see that the correction with $m_{\Pi_t}=150$ GeV is significantly smaller than those with larger m_{Π_t}. This is due to the $t\bar{b}$ threshold effect in the Π_t resonance contribution. For $\sqrt{s}=0.5$ TeV, we see from Table II that the relative correction $\Delta\sigma_{\Pi_t}/\sigma_0$ is around 0.1% if m_{Π_t} is smaller than the threshold and around (2–4)% if m_{Π_t} is larger than the threshold. For $\sqrt{s}=1.6$ TeV, $\Delta\sigma_{\Pi_t}/\sigma$ is around (0.3–0.8)%. These technicolor PGB corrections are quite small compared with those in the neutral channel $\gamma\gamma\to t\bar{t}$ [17]. This is because the contributions of Fig. 2(b), Fig. 2(c) and Fig. 2(d), Fig. 2(e) are destructive, which makes the charged channel very different from the neutral channel. With the integrated luminosity in Eq. (26), we see from the values of σ in Table II that, for a four-year run, there can be about $\approx$7000 events for $\sqrt{s}=0.5$ TeV, and $\geqslant$30000 events for $\sqrt{s}=1.6$ TeV. The corresponding statistical uncertainties at the 95% C.L. are then 2% for $\sqrt{s}=0.5$ TeV, and $\lesssim$1% for $\sqrt{s}=1.6$ TeV. Thus the effect of the top-pion corrections can hardly be experimentally detected if m_{Π_t} is smaller than the threshold and for $\sqrt{s}=1.6$ TeV, but *there is a possibility of detecting the signal for* $\sqrt{s}=0.5$ *TeV if* m_{Π_t} *is larger than the threshold* in the

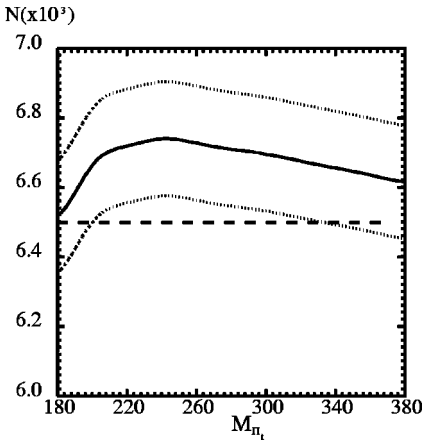

FIG. 4. The number of events N (4-year run at the TESLA) versus M_{Π_t} for $m_t'=5$ GeV and $M_\Pi=220$ GeV at $\sqrt{s}=0.5$ TeV in model TC2-I. The solid line is the total number of events, the dashed line is the number of events corresponding to the tree-level standard model contribution, and the dotted lines indicate the statistical uncertainty bounds at 95% C.L.

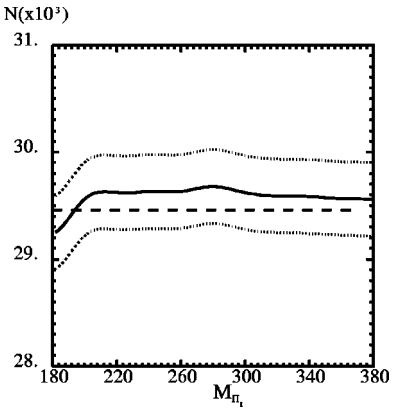

FIG. 5. The number of events N (4-year run at the TESLA) versus M_{Π_t} for $m_t'=5$ GeV and $M_\Pi=220$ GeV at $\sqrt{s}=1.6$ TeV in model TC2-I. The solid line is the total number of events, the dashed line is the number of events corresponding to the tree-level standard model contribution, and the dotted lines indicate the statistical uncertainty bounds at 95% C.L.

sense of statistical uncertainty.[3] To show the above results more intuitively, we plot, in Fig. 4 and Fig. 5, the number of events in a four-year run of the DESY TESLA at 0.5 TeV and 1.6 TeV, respectively, with m_{Π_t} in the range 180 GeV $\lesssim m_{\Pi_t} \lesssim$ 380 GeV. In the figures, the solid line stands for the total number of events, the dashed line stands for the number of events corresponding to the tree-level standard model contribution, and the dotted lines indicate the bounds of the statistical uncertainty at the 95% C.L. We see that the signal of Π_t contribution can possibly be detected in the range 200 GeV $\lesssim m_{\Pi_t} \lesssim$ 320 GeV at $\sqrt{s}=$ 0.5 TeV, while it cannot be detected at the 95% C.L. at $\sqrt{s}=$ 1.6 TeV.

In model TC2-II, the top-pion contributions are similar, while the Π^+ contributions are more significant than that in model TC2-I due to the smallness of F_Π in model TC2-II. The numerical results in model TC2-II are listed in Table III with the same ranges of m_{Π_t} and m_t', and with $m_\Pi=100$ and 220 GeV at the $\sqrt{s}=0.5$ TeV and $\sqrt{s}=1.6$ TeV LC. We see that the corrections are also significantly different for m_{Π_t} lying below or above the threshold. We see from Table III that the effect of Π^+ contributions, $\Delta\sigma_\Pi$, is negligibly small for $m_\Pi=100$ GeV, while is almost dominant for $m_\Pi=220$ GeV due to the effect of the tail of the Π^+-resonance. Take the $m_t'=5$ GeV case as an example. For $m_\Pi=220$ GeV, the relative correction $\Delta\sigma/\sigma$ ($\Delta\sigma \equiv \Delta\sigma_{\Pi_t}+\Delta\sigma_\Pi$) is around 16% for $\sqrt{s}=0.5$ TeV and is around 10% for $\sqrt{s}=1.6$ TeV, both for m_{Π_t} smaller or larger than the threshold, i.e. the corrections are much larger in this model due to the Π^+ contributions. For $m_\Pi=220$ GeV, the relative difference between the cross sections in model TC2-II and model TC2-I $[\sigma(\text{TC2-II})-\sigma(\text{TC2-I})]/\sigma(\text{TC2-I})$ is about 15% when $\sqrt{s}=0.5$ TeV and about 12% when $\sqrt{s}=1.6$ TeV. In this example, the number of events in a four-year run are about 7800 for $\sqrt{s}=0.5$ TeV, and about 33000 for $\sqrt{s}=1.6$ TeV. The corresponding statistical uncertainties at the 95% C.L. are then 2% for $\sqrt{s}=0.5$ TeV and 1% for $\sqrt{s}=1.6$ TeV. Thus the effect of the technicolor corrections in model TC2-II can be clearly detected both at the $\sqrt{s}=0.5$ TeV and $\sqrt{s}=1.6$ TeV energies. The difference between models TC2-I and TC2-II can also be clearly detected at $\sqrt{s}=0.5$, 1.6 TeV. So we conclude that *models* TC2-I and TC2-II can even be experimentally distinguished at the $\sqrt{s}=0.5$, 1.6 TeV TESLA via $e^+\gamma\to t\bar{b}\nu_e$ if m_Π is around 220 GeV. The plots corresponding to Fig. 4 and Fig. 5 for model TC2-II are given in Fig. 6 and Fig. 7, respectively.

As has been mentioned in Sec. II 2, the special arrangement of F_Q and F_L in the Appelquist-Terning one-family walking technicolor model causes that the color-singlet technipions are mainly composed of the technileptons, so that they do not couple to $t\bar{b}$. Thus there is no $t\bar{b}$-channel PGB contribution to the production cross section, and the technicolor corrections are only from the diagrams in Fig. 3 which are negligibly small. Numerical calculation shows that the relative correction is smaller than 1%. So the effect of the technicolor corrections cannot be detected via the process $e^+\gamma\to t\bar{b}\nu_e$. This is significantly different from the above two top-color-assisted technicolor models.

IV. CONCLUSIONS

In this paper, we have studied the possibility of testing different currently interesting improved technicolor models

[3]Since the ordinary one-loop radiative corrections, such as the contributions from Fig. 3(a)–Fig. 3(i), are already less than 1%, the theoretical uncertainty of this calculation (higher loop effects) is expected to be unimportant relative to the statistical uncertainty. A practical analysis of the detectability concerns also the systematic error and the detection efficiency in the experiments, but this is beyond the scope of this paper.

TABLE III. Top-pion and technipion corrections to the $e^+\gamma\to t\bar{b}\nu_e$ production cross section $\Delta\sigma_{\Pi_t}$,$\Delta\sigma_{\Pi}$ and the total production cross section $\sigma=\sigma_0+\Delta\sigma_{\Pi_t}+\Delta\sigma_{\Pi}$ in model TC2-II with $\sqrt{s}=0.5$, 1.6 TeV and various values of m_{Π_t},m_{Π},m_t'. The tree level production cross section $\sigma_0=3.25$ fb for $\sqrt{s}=0.5$ TeV, $\sigma_0=14.73$ fb for $\sqrt{s}=1.6$ TeV.

$\sqrt{s}$	m_{Π}	m_{Π_t}	$m_t'=5$ GeV			$m_t'=20$ GeV		
(TeV)	(GeV)	(GeV)	$\Delta\sigma_{\Pi_t}$ (fb)	$\Delta\sigma_{\Pi}$ (fb)	σ (fb)	$\Delta\sigma_{\Pi_t}$ (fb)	$\Delta\sigma_{\Pi}$ (fb)	σ(fb)
		150	0.0025		3.25	−0.004		3.25
		180	0.0083		3.26	0.006		3.26
	100	200	0.081	−0.0007	3.33	0.062	−0.0008	3.31
		240	0.12		3.37	0.096		3.35
		300	0.098		3.35	0.083		3.33
		380	0.058		3.31	0.052		3.30
0.5		150	0.0025		3.77	−0.004		6.63
		180	0.0083		3.78	0.006		6.64
	220	200	0.081	0.52	3.85	0.062	3.38	6.71
		240	0.12		3.89	0.096		6.75
		300	0.098		3.87	0.083		6.73
		380	0.058		3.83	0.052		6.69
		150	−0.12		14.56	−0.11		14.46
		180	−0.11		14.57	−0.099		14.47
	100	200	0.05	−0.047	14.73	0.039	−0.16	14.61
		240	0.086		14.77	0.061		14.63
		300	0.082		14.76	0.058		14.63
		380	0.05		14.73	0.042		14.61
1.6		150	−0.12		16.39	−0.11		26.14
		180	−0.11		16.40	−0.099		26.15
	220	200	0.05	1.78	16.56	0.039	11.53	26.31
		240	0.086		16.60	0.061		26.35
		300	0.082		16.59	0.058		26.34
		380	0.05		16.56	0.042		26.31

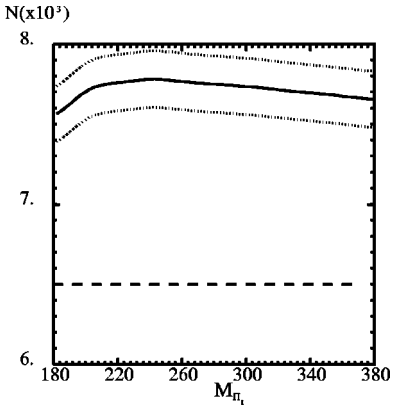

FIG. 6. The number of events N (4-year run at the TESLA) versus M_{Π_t} for $m_t'=5$ GeV and $M_{\Pi}=220$ GeV at $\sqrt{s}=0.5$ TeV in model TC2-II. The solid line is the total number of events, the dashed line is the number of events corresponding to the tree-level standard model contribution, and the dotted lines indicate the statistical uncertainty bounds at 95% C.L.

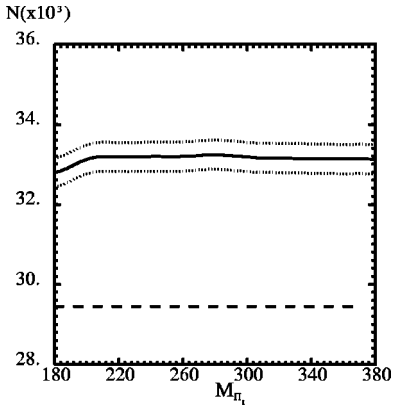

FIG. 7. The number of events N (4-year run at the TESLA) versus M_{Π_t} for $m_t'=5$ GeV and $M_{\Pi}=220$ GeV at $\sqrt{s}=1.6$ TeV in model TC2-II. The solid line is the total number of events, the dashed line is the number of events corresponding to the tree-level standard model contribution, and the dotted lines indicate the statistical uncertainty bounds at 95% C.L.

in the process $e^+\gamma\to t\bar{b}\bar{\nu}_e$ at the $\sqrt{s}=0.5$ TeV and $\sqrt{s}=1.6$ TeV LC, especially the DESY TESLA, via the effects of their typical PGB's. We see that the $t\bar{b}$-channel PGB contributions play dominant roles in this production process and their effects are experimentally detectable for certain reasonable parameter range in the sense of the statistical uncertainty. However, due to the destructive nature of the contributions of Fig. 2(b), Fig. 2(c) and Fig. 2(d), Fig. 2(e), the relative corrections in this charged channel are much smaller than those in the neutral channel $\gamma\gamma\to t\bar{t}$ [17], so that larger integrated luminosity is needed in the detection.

Specifically, in a four-year run of the DESY TESLA, the effects of the $t\bar{b}$-channel PGB's in models TC2-I and TC2-II are all experimentally detectable for reasonable parameter range, and these models can be experimentally distinguished through the differences of their cross sections. The Appelquist-Terning model, as a typical example of models without a $t\bar{b}$-channel PGB, is not detectable in the $e^+\gamma\to t\bar{b}\bar{\nu}_e$ process at the LC. Thus the $e^+\gamma\to t\bar{b}\bar{\nu}_e$ process at the LC provides a feasible test of the $t\bar{b}$-channel charged PGB's in various technicolor models.

Since the recent Fermilab CDF data on $t\bar{t}$ production at the Fermilab Tevatron show that the branching fraction for a top quark decaying into a final state e or μ is consistent with the standard model prediction up to certain uncertainty [18], a charged top-pion lighter than the top quark may not be favored [8], and a charged top-pion heavier than the top quark will have a braod width so that it is difficult to detect directly. Our results in model TC2-I show that the $e^+\gamma\to t\bar{b}\bar{\nu}_e$ process at the DESY TESLA provides feasible tests of the charged top-pion effect.

ACKNOWLEDGMENTS

This work is supported by the National Natural Science Foundation of China, the Fundamental Research Foundation of Tsinghua University, and a special grant from the State Commission of Education of China.

APPENDIX

Here we give the explicit expressions for $\Gamma^{(2b)}_{\mu\nu}(\Pi)$, $\Gamma^{(2c)}_{\mu\nu}(\Pi)$, $\Gamma^{(2d)}_{\mu\nu}(\Pi)$, $\Sigma_\rho(\Pi)$, $\Gamma^{(2b)}_{\mu\nu}(\Pi_t)$, $\Gamma^{(2c)}_{\mu\nu}(\Pi_t)$, $\Gamma^{(2d)}_{\mu\nu}(\Pi_t)$, and $\Sigma_\rho(\Pi_t)$ which can be obtained by direct calculations of the Feynman diagrams in Figs. 2(c)–2(e). The explicit expressions are

$$\Gamma^{(2b)}_{\mu\nu}(\Pi)=-c_f\frac{M_W m_t m_t'}{12\pi^2 F_\Pi}\sqrt{2\sqrt{2}\pi G_F\alpha}\{2[(p_{e^+}-p_{\bar{\nu}_e})_\mu(p_{e^+}-p_{\bar{\nu}_e})_\nu C_{21}+p_{\gamma\mu}p_{\gamma\nu}C_{22}+(p_{e^+}-p_{\bar{\nu}_e})_\mu p_{\gamma\nu}C_{23}+p_{\gamma\mu}$$
$$\times(p_{e^+}-p_{\bar{\nu}_e})_\nu C_{23}+g_{\mu\nu}C_{24}]-g_{\mu\nu}B_0(p_\gamma,m_b,m_b)-g_{\mu\nu}m_t^2C_0+(2p_{e^+}-2p_{\bar{\nu}_e}+p_\gamma)_\mu(p_{e^+}C_{11}-p_{\bar{\nu}_e}C_{11}+p_\gamma C_{12})_\nu$$
$$+(p_{e^+}C_{11}-p_{\bar{\nu}_e}C_{11}+p_\gamma C_{12})_\mu(2p_{e^+}-2p_{\bar{\nu}_e}+p_\gamma)_\nu-(p_{e^+}C_{11}-p_{\bar{\nu}_e}C_{11}+p_\gamma C_{12})^\rho(2p_{e^+\rho}g_{\mu\nu}-2p_{\bar{\nu}_e\rho}g_{\mu\nu}+p_{\gamma\rho}g_{\mu\nu}$$
$$+i\varepsilon_{\mu\rho\nu\sigma}p_\gamma^\sigma)+[2(p_{e^+}-p_{\bar{\nu}_e})_\mu(p_{e^+}-p_{\bar{\nu}_e})_\nu-(p_{e^+}-p_{\bar{\nu}_e})^2g_{\mu\nu}+(p_{e^+}-p_{\bar{\nu}_e})_\mu p_{\gamma\nu}-g_{\mu\nu}p_{e^+}.p_\gamma+g_{\mu\nu}p_{\bar{\nu}_e}.p_\gamma$$
$$+p_{\gamma\mu}(p_{e^+}-p_{\bar{\nu}_e})_\nu-i\varepsilon_{\mu\rho\nu\sigma}(p_{e^+}-p_{\bar{\nu}_e})^\rho p_\gamma^\sigma]C_0\}, \tag{A1}$$

$$\Gamma^{(2c)}_{\mu\nu}(\Pi)=c_f\frac{M_W m_t m_t'}{6\pi^2 F_\Pi}\sqrt{2\sqrt{2}\pi G_F\alpha}\{2[(p_{e^+}-p_{\bar{\nu}_e})_\mu(p_{e^+}-p_{\bar{\nu}_e})_\nu C_{21}^*+p_{\gamma\mu}p_{\gamma\nu}C_{22}^*+(p_{e^+}-p_{\bar{\nu}_e})_\mu p_{\gamma\nu}C_{23}^*+p_{\gamma\mu}$$
$$\times(p_{e^+}-p_{\bar{\nu}_e})_\nu C_{23}^*+g_{\mu\nu}C_{24}^*]+(p_{e^+}C_{11}^*-p_{\bar{\nu}_e}C_{11}^*+p_\gamma C_{12}^*)_\mu(2p_{e^+}-2p_{\bar{\nu}_e}+p_\gamma)_\nu-p_{\gamma\mu}(p_{e^+}C_{11}^*-p_{\bar{\nu}_e}C_{11}^*+p_\gamma C_{12}^*)_\nu$$
$$+g_{\mu\nu}(p_{e^+}.p_\gamma C_{11}^*-p_{\bar{\nu}_e}.p_\gamma C_{11}^*)-i\varepsilon_{\mu\rho\sigma\nu}[(p_{e^+}-p_{\bar{\nu}_e})C_{11}^*+p_\gamma C_{12}^*]^\rho p_\gamma^\sigma\}, \tag{A2}$$

$$\Gamma^{(2d)}_{\mu\nu}=c_f\frac{M_W m_t m_t'}{4\pi^2 F_\Pi}\sqrt{2\sqrt{2}\pi G_F\alpha}\times\frac{B_1(p_t+p_{\bar{b}},m_t,m_b)+B_0(p_t+p_{\bar{b}},m_t,m_b)}{M_W^2}$$
$$\times\{(p_{e^+}-p_{\bar{\nu}_e})_\mu(p_{e^+}-p_{\bar{\nu}_e})_\nu-p_{\gamma\mu}p_{\gamma\nu}-g_{\mu\nu}(p_{e^+}-p_{\bar{\nu}_e})^2\}, \tag{A3}$$

$$-i\Sigma_\mu(\Pi)=c_f\frac{M_W m_t m_t'}{8\pi^2 F_\Pi}\sqrt{2\sqrt{2}G_F}(p_t+p_{\bar{b}})_\mu\{B_1(p_t+p_{\bar{b}},m_t,m_b)+B_0(p_t+p_{\bar{b}},m_t,m_b)\}, \tag{A4}$$

$$C_{ij}=C_{ij}(p_{\bar{\nu}_e}-p_{e^+},-p_\gamma,m_t,m_b,m_b),$$

$$C_{ij}^*=C_{ij}(p_{e^+}-p_{\bar{\nu}_e},p_\gamma,m_b,m_t,m_t), \tag{A5}$$

where C_{ij}'s are the standard 3-point functions given in Ref. [27].

The expressions for $\Gamma_{\mu\nu}^{(2b)}(\Pi_t)$, $\Gamma_{\mu\nu}^{(2c)}(\Pi_t)$, $\Gamma_{\mu\nu}^{(2d)}(\Pi_t)$, and $\Sigma_\mu(\Pi_t)$ can be obtained by simply replacing m_t' by $m_t - m_t'$, F_Π by F_{Π_t} and taking $c_f=1$.

[1] S. Weinberg, Phys. Rev. D **13**, 974 (1976); **19**, 1277 (1979); L. Susskind, *ibid.* **20**, 2619 (1979); S. Dimopoulos and L. Susskind, Nucl. Phys. **B155**, 237 (1979); E. Eichten and K. Lane, Phys. Lett. **90B**, 125 (1980).

[2] M. Peskin and T. Takeuchi, Phys. Rev. Lett. **65**, 964 (1990).

[3] J. Erler and P. Langacker, in Review of Particle Physics, Eur. Phys. J. C **3**, 90 (1998).

[4] K. Hagiwara, D. Haidt, and S. Matsumoto, Eur. Phys. J. C **2**, 95 (1998).

[5] B. Holdom, Phys. Rev. D **24**, 1441 (1981); Phys. Lett. **150B**, 301 (1985); T. Appequist and L.C.R. Wijewardhana, Phys. Rev. D **36**, 568 (1987); K. Yamawaki, M. Banda, and K. Matsumoto, Phys. Rev. Lett. **56**, 1335 (1986); T. Akiba and T. Yanagida, Phys. Lett. **169B**, 432 (1986).

[6] T. Appelquist and J. Terning, Phys. Lett. B **315**, 139 (1993).

[7] K. Lane and E. Eichten, Phys. Lett. B **222**, 274 (1989); K. Lane and M.V. Ramana, Phys. Rev. D **44**, 2678 (1991).

[8] C.T. Hill, Phys. Lett. B **345**, 483 (1995);

[9] K. Lane and E. Eichten, Phys. Lett. B **352**, 382 (1995); K. Lane, Phys. Rev. D **54**, 2204 (1996); K. Lane, Proceedings of the 1996 Workshop on Perspectives of Strongly Coupled Gauge Theories, Nagoya, Japan, Boston University Report No. BUHEP-97-8, p. 72.

[10] See, for example, E.H. Simmons, R.S. Chivukula, and J. Terning, in *Heavy Flavor and Electroweak Theory*, Proceedings of the International Symposium, Beijing, China, edited by C.-H. Chang and C.-S. Huang (World Scientific, Singapore, 1995), pp. 234–243.

[11] CDF Collaboration, F. Abe *et al.*, Phys. Rev. Lett. **74**, 2626 (1995); D0 Collaboration, S. Abachi *et al.*, *ibid.* **74**, 2632 (1995); Particle Data Group, C. Caso *et al.*, Eur. Phys. J. C **3**, 1 (1998).

[12] For example, F. Larios and C.-P. Yuan, Phys. Rev. D **55**, 7218 (1997); F. Larios, E. Malkawi, and C.-P. Yuan, in *Physics at TeV Energy Scale* (CCAST-WL Workshop Series: Vol. 72), edited by Yu-Ping Kuang (CCAST, Beijing, China, 1996), pp. 49–118.

[13] For example, T. Han, K. Whisnant, B.-L. Young, and X. Zhang, Phys. Lett. B **385**, 311 (1996); Phys. Rev. D **55**, 7241 (1997); M. Hosch, K. Whisnant, and B.-L. Young, Iowa State Univ. Report No. AMES-HET-96-04; K.J. Abraham, K. Whisnant, and B.-L. Young, Report No. AMES-HET-97-07; R.J. Oakes, K. Whisnant, J.M. Yang, B.-L. Young, and X. Zhang, Report No. AMES-HET-97-08.

[14] E. Boos, A. Pukhov, M. Sachwitz, and H.J. Schreiber, DESY Preprint DESY 97-123E, hep-ph/9711253.

[15] For example, J.M. Yang and C.S. Li, Phys. Rev. D **52**, 1541 (1995); C.H. Chang, C.S. Li, R.J. Oakes, and J.M. Yang, *ibid.* **51**, 2125 (1995); C.S. Li and J.M. Yang, in *Heavy Flavor and Electroweak Theory* (Ref. [10]), pp. 276–285 and references therein; C.S. Li, J.M. Yang, Y.L. Zhu, and H.Y. Zhou, Phys. Rev. D **54**, 4662 (1996); H.Y. Zhou and C.S. Li, *ibid.* **55**, 4421 (1996); C.S. Li, H.Y. Zhou, Y.L. Zhu, and J.M. Yang, Phys. Lett. B **379**, 135 (1996); H. Wang, C.S. Li, H.Y. Zhou, and Y.P. Kuang, Phys. Rev. D **54**, 4374 (1996).

[16] E. Eichten and K. Lane, Phys. Lett. B **327**, 129 (1994); C. Hill and S. Parke, Phys. Rev. D **49**, 4454 (1994); S. Parke, in *Heavy Flavor and Electroweak Theory* (Ref. [10]), pp. 273–275; C.-X. Yue, H.-Y. Zhou, Y.-P. Kuang, and G.-R. Lu, Phys. Rev. D **55**, 5541 (1997).

[17] H.-Y. Zhou, Y.-P. Kuang, C.-X. Yue, H. Wang, and G.-R. Lu, Phys. Rev. D **57**, 4205 (1998).

[18] T. Stelzer and S. Willenbrock, Phys. Lett. B **357**, 125 (1995).

[19] For example, R.S. Chivukula, S.B. Selipsky, and E.H. Simmons, Phys. Rev. Lett. **69**, 575 (1992); R.S. Chivukula, E. Gates, E.H. Simmons, and J. Terning, Phys. Lett. B **311**, 575 (1992); N. Evans, *ibid.* **331**, 378 (1994); E.H. Simmons, Boston Univ. Report No. BUHEP-96-37; C.-X. Yue, Y.-P. Kuang, and G.-R. Lu, Phys. Rev. D **56**, 291 (1997); G.-R. Lu, Y.-G. Cao, and X.-L. Wang, *ibid.* **56**, 135 (1997).

[20] CDF Collaboration, F. Abe *et al.*, Phys. Rev. Lett. **80**, 2773 (1998).

[21] R.S. Chivukula, B.A. Dobrescu, and J. Terning, Phys. Lett. B **353**, 289 (1995); D. Kominis, *ibid.* **358**, 312 (1995); G. Buchalla, G. Burdman, C.T. Hill, and D. Kominis, Phys. Rev. D **53**, 5185 (1996).

[22] Chong-Xing Yue, Yu-Ping Kuang, and Gong-Ru Lu, Phys. Rev. D **56**, 291 (1997).

[23] V. Lubicz and P. Santorelli, Nucl. Phys. **B460**, 3 (1996).

[24] S. Adler, Phys. Rev. **177**, 2426 (1969); J.S. Bell and R. Jackiw, Nuovo Cimento A **60**, 47 (1969).

[25] J. Ellis, M.K. Gaillard, D.V. Nanopoulos, and P. Sikivie, Nucl. Phys. **B182**, 529 (1981).

[26] B. Balaji, Phys. Rev. D **53**, 1699 (1996).

[27] G. Passarino and M. Veltman, Nucl. Phys. **B160**, 151 (1979); A. Axelrod, *ibid.* **B209**, 349 (1982); M. Clements *et al.*, Phys. Rev. D **27**, 570 (1983).

[28] K. Lane, Phys. Lett. B **357**, 624 (1995).

[29] G. Jikia, Nucl. Phys. **B374**, 83 (1992).
[30] K. Hagiwara and D. Zeppenfeld, Nucl. Phys. **B313**, 560 (1989); V. Barger, T. Han, and D. Zeppenfeld, Phys. Rev. D **41**, 2782 (1990).
[31] A. Denner, Fortschr. Phys. **41**, 307 (1994).
[32] W. Beenakker *et al.*, Nucl. Phys. **B411**, 343 (1994).
[33] J.F. Donoghue, E. Golowich, and B.R. Holstein, *Dynamics of the Standard Model* (Cambridge Univiversity Press, Cambridge, England, 1992), p. 34.
[34] P.M. Zerwas (private communication).